IOP Publishing Physica Scripta
Phys. Scr. 95 (2020) 024001 (10pp) https://doi.org/10.1088/1402-4896/ab456b

Interplay between shape-phase transitions and shape coexistence in the Zr isotopes

N Gavrielov[1,3], A Leviatan[1] and F Iachello[2]

[1] Racah Institute of Physics, The Hebrew University, Jerusalem 91904, Israel
[2] Center for Theoretical Physics, Sloane Physics Laboratory, Yale University, New Haven, CT 06520-8120, United States of America

E-mail: noam.gavrielov@mail.huji.ac.il, ami@phys.huji.ac.il and francesco.iachello@yale.edu

Received 18 July 2019, revised 12 September 2019
Accepted for publication 17 September 2019
Published 31 December 2019

Abstract

We investigate the evolution of structure in the zirconium isotopes where one of the most complex situations encountered in nuclear physics occurs. We demonstrate the role of two concurrent types of quantum phase transitions, sharing a common critical point. The first type, involves an abrupt crossing of coexisting normal and intruder configurations. The second type, involves a gradual shape-phase transition within the intruder configuration, changing from weakly-deformed to prolate-deformed and finally to gamma-unstable. Evidence for this scenario is provided by a detailed comparison with experimental data, using a definite algebraic framework.

Keywords: quantum phase transitions in nuclei, nuclear shape-phase transitions, nuclear shape coexistence, Zr isotopes, interacting boson model of nuclei

(Some figures may appear in colour only in the online journal)

1. Introduction

Nuclei in the $Z \approx 40$, $A \approx 100$ region have long been recognized to exhibit an abrupt transition from spherical to deformed ground states and the emergence of shape-coexisting states [1–3]. From a shell-model perspective, the sudden onset of deformation at neutron number 60, has been ascribed to a strong isoscalar proton-neutron interaction between nucleons occupying the $1g_{9/2}$-$1g_{7/2}$ spin-orbit partners [2–5], producing a crossing of normal and intruder configurations (the latter arising from the promotion of two protons across the $Z = 40$ sub-shell gap). These dramatic structural changes have attracted considerable theoretical and experimental interest. In the Zr chain, they have been studied in a variety of theoretical approaches, including mean-field based methods, both non-relativistic [6, 7] and relativistic [8], large-scale shell model calculations [9, 10] and the Monte-Carlo shell-model (MCSM) [11]. The Zr isotopes have been recently the subject of several experimental investigations [12–18], opening the door for understanding the properties of both yrast and non-yrast states.

Qualitative changes in the ground state properties of a physical system, induced by a variation of parameters in the quantum Hamiltonian, are called quantum phase transitions (QPTs) [19, 20]. The latter have in recent years become of great interest in a variety of fields [21]. In nuclei, examples of QPTs are shape changes within a single configuration, as observed in the neutron number 90 region for Nd–Sm–Gd isotopes [22], and shape coexistence involving multiple configurations, as observed in nuclei near shell closure, e.g. the light Pb–Hg isotopes [5], with strong mixing between the configurations.

In the present work, we show that these different types of QPTs [23] play a role in the Zr chain, and that in parallel to an abrupt swapping of configurations, each configuration maintains its purity and its own gradual shape-evolution with nucleon number. This situation, referred to as intertwined QPTs [24], gives rise to an intricate interplay between shape-phase transitions and shape coexistence in nuclei.

The notion of intertwined QPTs is illustrated schematically in figure 1, where a sudden crossing of two configurations versus nucleon number is superimposed on progressive shape-changes in each configuration. In what follows, we provide evidence for such a scenario in the Zr isotopes by means of a detailed comparison with experimental data, analyzed in a physically transparent symmetry-based framework, the interacting boson model (IBM) [25]. After a brief

[3] Author to whom any correspondence should be addressed.

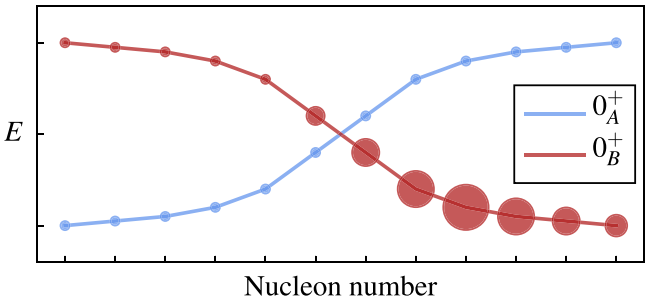

Figure 1. Schematic illustration of the scenario of intertwined quantum phase transitions. The evolution with nucleon number of energies (in arbitrary units) of the lowest 0^+ states of two configurations, *A* and *B*, discloses an abrupt crossing. This change in configurations is accompanied by gradual changes of shapes (denoted by circles of different size) within each configuration.

review in section 2 of the model and its extensions to accommodate configuration mixing, we apply the formalism to the Zr chain in section 3 and present both a quantum and a classical analysis. In section 4 we discuss the evolution of the quantum spectra with nucleon number, identifying the underlying multiple QPTs. In section 5 we present the corresponding evolution of order parameters and related observables, including *E*2 transition rates, isotope shifts and two-neutron separation energies. Concluding remarks are collected in section 6.

2. QPTs in the IBM and its extensions

The IBM describes low lying quadrupole states in even–even nuclei in terms of a system of monopole (s) and quadrupole (d) bosons, representing valence nucleon pairs [25, 26]. For a single shell-model configuration space, the total number of bosons is conserved and is fixed by the microscopic interpretation to be $N = N_\pi + N_\nu$, where N_π (N_ν) is the number of proton (neutron) particle or hole pairs counted from the nearest closed shell. In its simplest version, the IBM has U(6) as a spectrum generating algebra and exhibits three dynamical symmetry (DS) limits with leading subalgebras: U(5), SU(3) and SO(6), whose analytic solutions resemble known paradigms of collective motion: spherical vibrator, axially-symmetric and γ-soft deformed rotors, respectively. A geometric visualization of the IBM is obtained by an energy surface,

$$E_N(\beta, \gamma) = \langle \beta, \gamma; N|\hat{H}|\beta, \gamma; N\rangle, \tag{1}$$

defined by the expectation value of the Hamiltonian in the following coherent (intrinsic) state [27, 28],

$$|\beta, \gamma; N\rangle = (N!)^{-1/2}(b_c^\dagger)^N|0\rangle, \tag{2a}$$

$$\begin{aligned} b_c^\dagger \;=\; & (1+\beta^2)^{-1/2}[\beta\cos\gamma\, d_0^\dagger \\ & + \beta\sin\gamma(d_2^\dagger + d_{-2}^\dagger)/\sqrt{2} \;+ s^\dagger]. \end{aligned} \tag{2b}$$

Here, (β, γ) are quadrupole shape parameters whose values, $(\beta_{\rm eq}, \gamma_{\rm eq})$, at the global minimum of $E_N(\beta, \gamma)$ define the equilibrium shape for a given Hamiltonian. For two body interactions, the shape can be spherical ($\beta_{\rm eq} = 0$) or deformed ($\beta_{\rm eq} > 0$) with $\gamma_{\rm eq} = 0$ (prolate), $\gamma_{\rm eq} = \pi/3$ (oblate), or γ-independent.

The DSs correspond to possible phases of the system. QPTs can be studied in the IBM using an Hamiltonian $\hat{H}(\xi)$ which interpolates between the DS limits (phases) by varying its control parameters ξ. The related energy surface $E_N(\beta, \gamma; \xi)$ serves as the Landau potential, whose topology determines the type of phase transition (Ehrenfest classification). The order parameter is taken to be the expectation value of the d-boson number operator, $\hat{n}_d$, in the ground state

$$\frac{\langle \hat{n}_d\rangle}{N} \approx \frac{\beta_{\rm eq}^2}{1+\beta_{\rm eq}^2}, \tag{3}$$

which in turn is related to the expectation value in $|\beta_{\rm eq}, \gamma_{\rm eq}; N\rangle$, hence to the equilibrium deformation, $\beta_{\rm eq}$. The dependence of $\beta_{\rm eq}$ on ξ, discloses the order of the transition.

QPTs involving a single configuration have been studied extensively in the IBM framework [22, 28–30]. A typical Hamiltonian frequently used in such studies, has the form [31, 32],

$$\hat{H}(\epsilon_d, \kappa, \chi) = \epsilon_d\, \hat{n}_d + \kappa\, \hat{Q}_\chi \cdot \hat{Q}_\chi, \tag{4}$$

where the quadrupole operator is given by

$$\hat{Q}_\chi = d^\dagger s + s^\dagger \tilde{d} + \chi(d^\dagger \times \tilde{d})^{(2)}. \tag{5}$$

Here, $\tilde{d}_m = (-1)^m d_{-m}$ and standard notation of angular momentum coupling is used. The associated Landau potential reads

$$\begin{aligned} & E_N(\beta, \gamma;\, \epsilon_d, \kappa, \chi) \\ & \quad = 5\kappa\, N + \frac{N\beta^2}{1+\beta^2}[\,\epsilon_d + \kappa(\chi^2 - 4)] \\ & \quad + \frac{N(N-1)\beta^2}{(1+\beta^2)^2}\kappa[\,4 - 4\bar{\chi}\beta\,\Gamma + \bar{\chi}^2\beta^2\,], \end{aligned} \tag{6}$$

where $\bar{\chi} = \sqrt{\frac{2}{7}}\chi$ and $\Gamma = \cos 3\gamma$. The control parameters $(\epsilon_d, \kappa, \chi)$ in equation (4), interpolate between the U(5), SU(3) and SO(6) DS limits, which are reached for $(\kappa = 0)$, $(\epsilon_d = 0,\ \chi = -\frac{\sqrt{7}}{2})$ and $(\epsilon_d = 0,\ \chi = 0)$, respectively. The U(5)-SU(3) transition is found to be first-order, the U(5)-SO(6) transition is second order and the SU(3)-SO(6) transition is a crossover.

An extension of the IBM to include intruder excitations is based on associating the different shell-model spaces of 0p-0h, 2p-2h, 4p-4h, … particle–hole excitations, with the corresponding boson spaces comprising of N, $N+2$, $N+4$, … bosons, which are subsequently mixed. The resulting IBM with configuration mixing (IBM-CM) [33, 34] has been used extensively for describing configuration-mixed QPTs and coexistence phenomena in nuclei [33–44]. In this case, the quantum Hamiltonian has a matrix form [39]

$$\hat{H}(\xi_A, \xi_B, \omega) = \begin{bmatrix} \hat{H}_A(\xi_A) & \hat{W}(\omega) \\ \hat{W}(\omega) & \hat{H}_B(\xi_B) \end{bmatrix}, \tag{7}$$

where the index A, B denote the two configurations. The Hamiltonian $\hat{H}_A(\xi_A)$ acts on the A (normal) configuration,

corresponding to the valence space and $\hat{H}_B(\xi_B)$ on the B (intruder) configuration, corresponding to the core-excited excitations. The $\hat{W}(\omega)$ term mixes both spaces. When two configurations coexist, the energy surface becomes a matrix

$$E(\beta, \gamma) = \begin{bmatrix} E_A(\beta, \gamma; \xi_A) & \Omega(\beta, \gamma; \omega) \\ \Omega(\beta, \gamma; \omega) & E_B(\beta, \gamma; \xi_B) \end{bmatrix}, \tag{8}$$

whose entries are the matrix elements of the corresponding terms in the Hamiltonian (7), between the intrinsic states (2) of the two configurations, with appropriate boson numbers. Diagonalization of this two-by-two matrix produces the so-called eigen-potentials, $E_{\pm}(\beta, \gamma)$ [39, 45, 46].

As the control parameters (ξ_A, ξ_B, ω) in the Hamiltonian (7) are varied, the two coexisting configurations can exchange roles, and their individual shapes can evolve. Usually the latter quantum shape-phase transitions are masked by the strong mixing between the two configurations. In what follows, we show that the Zr isotopes are exceptional in the sense that the crossing is abrupt, the separate configurations retain their purity before and after the crossing, and the shape evolution of the intruder configuration can be cast in terms of its own phase transition.

3. The IBM-CM in the Zr chain

To describe the $_{40}$Zr isotopes in the IBM-CM framework, requires a choice of Hilbert space, Hamiltonian and transition operators. Similar to a calculation done for the $_{42}$Mo isotopes in [35], we consider $^{90}_{40}Zr_{50}$ as a core and valence neutrons in the 50–82 major shell. The normal A-configuration corresponds to having no active protons above $Z = 40$ sub-shell gap, and the intruder B-configuration corresponds to two-proton excitation from below to above this gap, creating 2p-2h states. According to the usual boson-counting, the corresponding bosonic configurations have proton bosons $N_\pi = 0$ for the normal configuration and $N_\pi = 2$ for the intruder configuration. Both configurations have neutron bosons $N_\nu = 1, 2, \ldots, 8$ for neutron number 52–66, and $\bar{N}_\nu = 7, 6$ for 68–70, where the bar over the number indicates that these are hole bosons. Altogether, the IBM-CM model space, employed in the current study, consists of a $[N] \oplus [N+2]$ boson space with total boson number $N = 1, 2, \ldots, 8$ for $^{92-106}$Zr and $\bar{N} = 7, 6$ for ^{108,110}Zr. These two configurations are shown in figure 2, for $^{100}_{40}Zr_{60}$.

We write the Hamiltonian not in the matrix form of equation (7), but rather in the equivalent form

$$\hat{H} = \hat{H}_A^{(N)} + \hat{H}_B^{(N+2)} + \hat{W}^{(N,N+2)}. \tag{9}$$

Here, $\hat{\mathcal{O}}^{(N)} = \hat{P}_N^\dagger \hat{\mathcal{O}} \hat{P}_N$ and $\hat{\mathcal{O}}^{(N,N')} = \hat{P}_N^\dagger \hat{\mathcal{O}} \hat{P}_{N'}$, for an operator $\hat{\mathcal{O}}$, with $\hat{P}_N$, a projection operator onto the $[N]$ boson space. The Hamiltonian $\hat{H}_A^{(N)}$ represents the normal (N boson space) configuration and $\hat{H}_B^{(N+2)}$ represents the intruder configuration ($N + 2$ boson space). The explicit form of these Hamiltonians is given by

$$\hat{H}_A = \hat{H}(\epsilon_d^{(A)}, \kappa^{(A)}, \chi), \tag{10a}$$

$$\hat{H}_B = \hat{H}(\epsilon_d^{(B)}, \kappa^{(B)}, \chi) + \kappa'^{(B)} \hat{L} \cdot \hat{L} + \Delta_p. \tag{10b}$$

They involve terms similar to those of the single-configuration Hamiltonian of equation (4). $\hat{H}_B$ of equation (10*b*), contains an additional rotational term and Δ_p is an off-set between the normal and intruder configurations, where the index p denotes the fact that this is a proton excitation. The mixing term in equation (9) has the form [25, 33, 34]

$$\hat{W} = \omega \left[(d^\dagger \times d^\dagger)^{(0)} + (s^\dagger)^2 \right] + \text{H.c.}, \tag{11}$$

where H.c. stands for Hermitian conjugate. The resulting eigenstates $|\Psi; L\rangle$ with angular momentum L, are linear combinations of the wave functions, Ψ_A and Ψ_B, in the two spaces $[N]$ and $[N + 2]$,

$$|\Psi; L\rangle = a|\Psi_A; [N], L\rangle + b|\Psi_B; [N+2], L\rangle, \tag{12}$$

with $a^2 + b^2 = 1$. The above decomposition reflects the normal-intruder mixing in the state considered.

Adapted to two configurations, the $E2$ operator reads

$$\hat{T}(E2) = e^{(A)} \hat{Q}_\chi^{(N)} + e^{(B)} \hat{Q}_\chi^{(N+2)}, \tag{13}$$

with $\hat{Q}_\chi^{(N)} = \hat{P}_N^\dagger \hat{Q}_\chi \hat{P}_N$, $\hat{Q}_\chi^{(N+2)} = P_{N+2}^\dagger \hat{Q}_\chi \hat{P}_{N+2}$, and $\hat{Q}_\chi$, defined in equation (5), is the same quadrupole operator appearing in the Hamiltonian. In equation (13), $e^{(A)}$ and $e^{(B)}$ are the boson effective charges for the configurations A and B, respectively.

A geometric interpretation is obtained by means of the matrix $E(\beta, \gamma)$, equation (8), with entries $E_A(\beta, \gamma) = \langle \beta, \gamma; N|\hat{H}_A|\beta, \gamma; N\rangle$, $E_B(\beta, \gamma) = \langle \beta, \gamma; N+2|\hat{H}_B|\beta, \gamma; N+2\rangle$ and $\Omega(\beta, \gamma) = \langle \beta, \gamma; N|\hat{W}|\beta, \gamma; N+2\rangle$. These entries involve the expectation values of the Hamiltonians $\hat{H}_A$ (10*a*) and $\hat{H}_B$ (10*b*), in the intrinsic states (2), with N and $N + 2$ bosons respectively, and a non-diagonal matrix element of the mixing term $\hat{W}$ (11), between them. The explicit expressions are found to be

$$E_A(\beta, \gamma) = E_N(\beta, \gamma; \epsilon_d^{(A)}, \kappa^{(A)}, \chi), \tag{14a}$$

$$E_B(\beta, \gamma) = E_{N+2}(\beta, \gamma; \epsilon_d^{(B)}, \kappa^{(B)}, \chi) + 6\kappa'^{(B)} \frac{(N+2)\beta^2}{1+\beta^2} + \Delta_p, \tag{14b}$$

$$\Omega(\beta, \gamma) = \frac{\sqrt{(N+2)(N+1)}}{1+\beta^2} \omega \left(1 + \frac{1}{\sqrt{5}} \beta^2 \right), \tag{14c}$$

where the surfaces on the right-hand-side of equations (14*a*)–(14*b*) are obtained from equation (6).

4. Quantum and classical analyses

A first step in a quantum analysis involves a numerical diagonalization of the IBM-CM Hamiltonian, and evaluating matrix elements of the $E2$ operator (13) between its eigenstates. The parameters of these operators are determined from a combined fit to the data on spectra and $E2$ transitions. The calculated observables are then compared with the measured values.

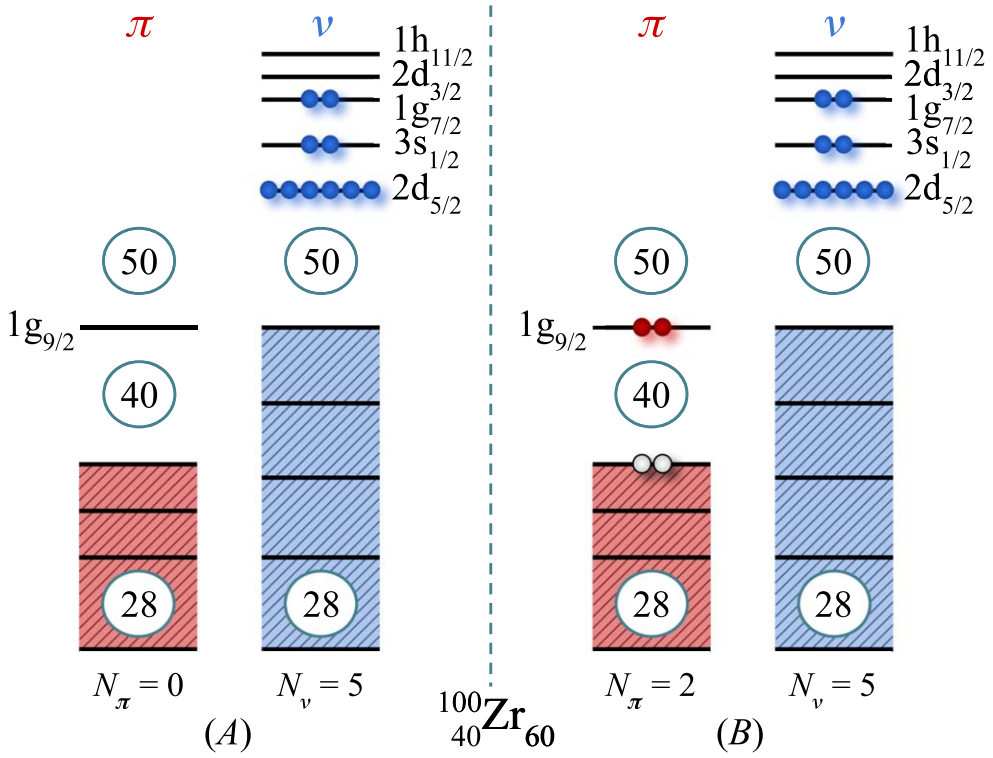

Figure 2. Schematic representation of the two coexisting shell-model configurations (*A* and *B*) for $^{100}_{40}Zr_{60}$. The corresponding numbers of proton bosons (N_π) and neutron bosons (N_ν), relevant to the IBM-CM, are listed for each configuration.

The adapted fitting procedure is similar to that used in [35–42]. We allow a gradual change of the parameters between adjacent isotopes, but take into account the proposed shell-model interpretation for the structure evolution in this region [2–4]. The Hamiltonian parameters used are displayed in figure 3 and are consistent with those of previous calculations in this mass region [35–37]. A symmetry about mid-shell, at neutron number 66, was imposed on all parameters (except χ), in accord with microscopic aspects of the IBM [26]. Apart from some fluctuations due to the subshell closure at neutron number 56 (the filling by the neutrons of the $2d_{5/2}$ orbital), the values of the parameters are a smooth function of neutron number and, in some cases, a constant. A notable exception is the sharp decrease by 1 MeV of the energy offset parameter Δ_p beyond neutron number 56. Such a behavior was observed for the Mo and Ge chains [35–37] and, as noted in [35], it reflects the effects of the isoscalar residual interaction, V_{pn}, between protons and neutrons occupying the partner orbitals $1g_{9/2}$ and $1g_{7/2}$, which is the established mechanism for descending cross shell-gap excitations and onset of deformation in this region [3, 4]. The trend in Δ_p agrees with shell model estimates for the monopole correction of V_{pn} [47]. The mixing parameter ω (11) is determined from $E2$ transitions between configurations, and is kept constant except for neutron numbers 52–54, where the normal configuration space is small ($N = 1, 2$). In general, the underlying physics in the current IBM study is similar to that of [3, 4], which albeit use a different formal language, in which the lowering in energy and developed collectivity of the intruder configuration are governed by the relative magnitude

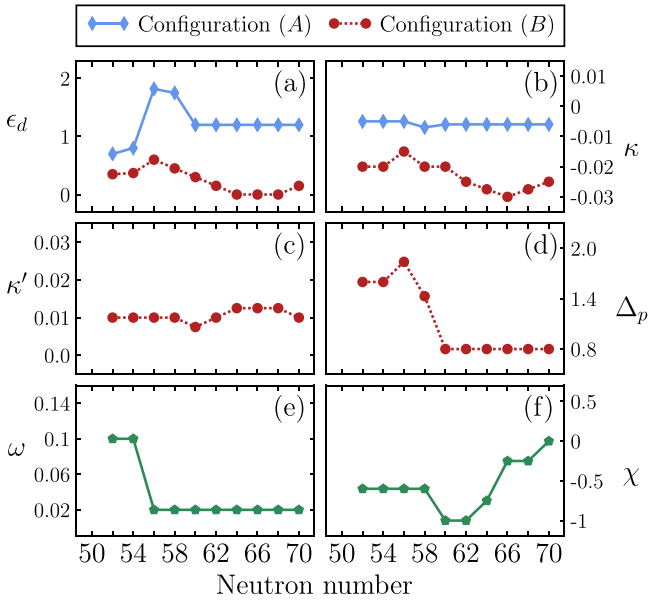

Figure 3. Parameters of the IBM-CM Hamiltonians, equations (10*a*), (10*b*), (11), are in MeV and the parameter χ of equation (5), is dimensionless.

of V_{pn} (especially its monopole and quadrupole components) and the energy gaps between spherical shell-model states near shell and subshell closures. A more direct relation between the two approaches necessitates a proton-neutron version of the IBM. The boson effective charges in the $E2$ operator (13), $e^{(A)} = 0.9$ and $e^{(B)} = 2.24$ (W.u.)$^{1/2}$, are determined from

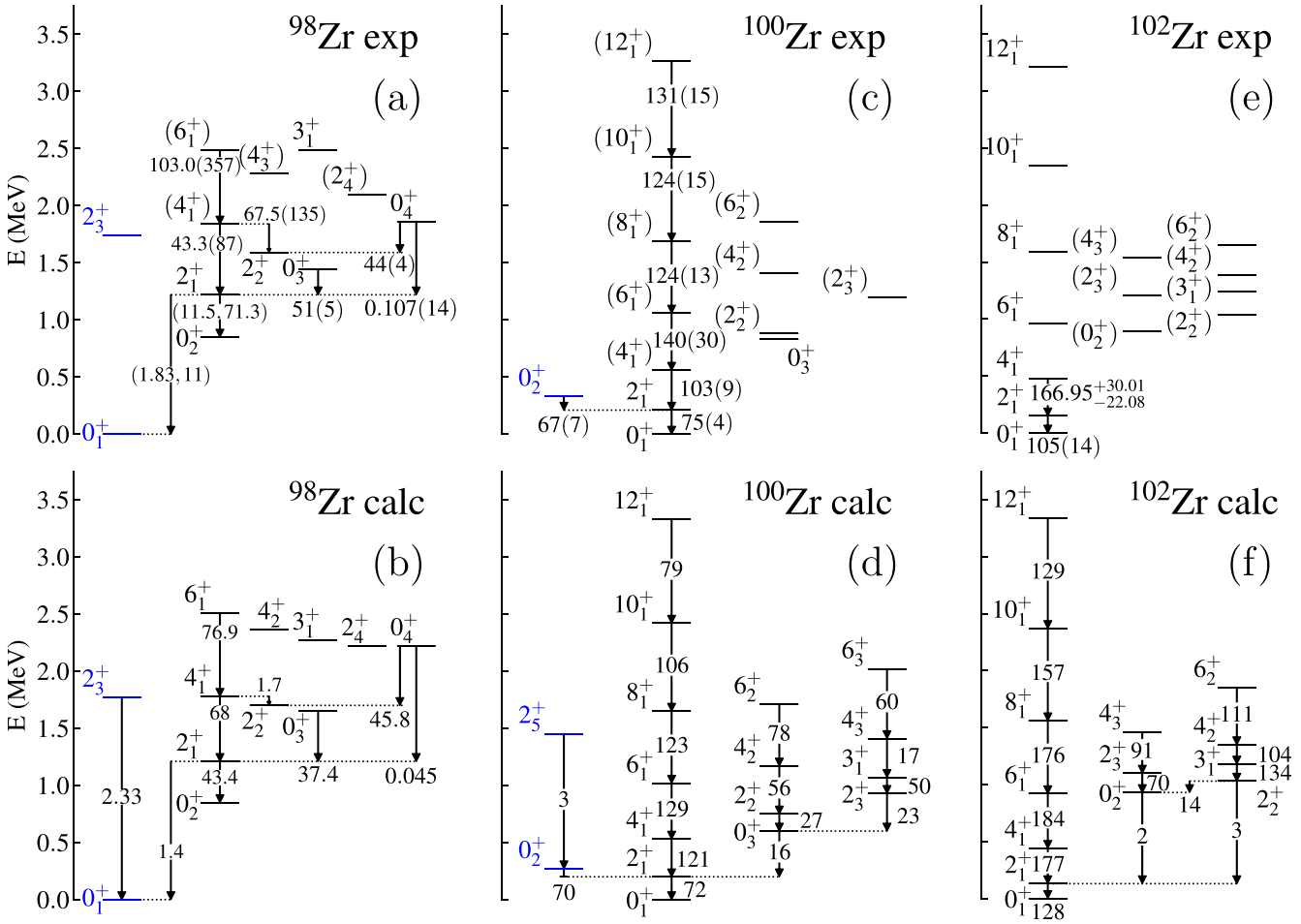

Figure 4. Experimental [15, 17, 18, 50] (top row) and calculated (bottom row) energy levels in MeV and $E2$ rates in W.u. for ^{98}Zr [panels (a)–(b)], ^{100}Zr [panels (c)–(d)] and ^{102}Zr [panels (e)–(f)]. The levels $(0_1^+, 2_3^+)$ in ^{98}Zr and $(0_2^+, 2_5^+)$ in ^{100}Zr are dominated by the normal (A) configuration. All other levels shown are dominated by the intruder (B) configuration. Assignments are based on the decomposition of equation (12).

the $2^+ \rightarrow 0^+$ transitions within each configuration and χ is the same parameter as in the Hamiltonian, shown in figure 3. Fine-tuning the parameters for individual isotopes can improve the fit, but the main conclusions of the analysis, to be reported below, are not changed.

The calculations describe the experimental data in the entire range $^{92-110}$Zr very well. A full account is given in [48]. Here we show only three examples, ^{98}Zr, ^{100}Zr and ^{102}Zr, where a first-order shape-phase transition takes place, accompanied by a crossing of the normal and intruder configurations. ^{98}Zr, in figures 4(a) and (b), has a spherical [U(5)-like] ground state configuration (A) and a weakly-deformed [U(5)-perturbed] excited configuration (B). ^{100}Zr is near the critical point of both types of phase transitions, and yet our description of energy levels and $B(E2)$ values is excellent; see figures 4(c) and (d). The ground state band, has now become configuration (B), and appears to have features of the so-called X(5) symmetry [49], while the spherical configuration (A) has now become the excited band 0_2^+. ^{102}Zr, in figure 4(e) and (f), exhibits well developed deformed [SU(3)-like] rotational bands assigned to configuration (B). States of configuration (A) have shifted to higher energies.

The assignment of a given state to the normal A-configuration or to the intruder B-configuration, can be inferred from the probabilities a^2 or b^2 of the decomposition, equation (12). The closest DS to the state considered, is determined by expanding its wave function in the U(5), SU(3) and SO(6) bases. Figure 5 shows the percentage of the wave function within the intruder configuration for the ground (0_1^+) and excited (0_2^+) states. The rapid change in structure of the 0_1^+ state from the normal A-configuration in ^{98}Zr to the intruder B-configuration in ^{100}Zr is clearly evident. The 0_2^+ state shows a similar behavior but with the roles of the two configurations exchanged. In ^{102}Zr both states belong to the intruder B-configuration.

One of the main advantages of the algebraic method employed, is that one can do both a quantum and a classical analysis. In figure 6, we show the calculated lowest eigenpotential $E_-(\beta, \gamma)$, which is the lowest eigenvalue of the two-by-two matrix (8), with elements given in equation (14). These classical potentials confirm the quantum results, as they show a transition from spherical ($^{92-98}$Zr), to a flat-bottomed potential at ^{100}Zr, to prolate axially-deformed ($^{102-104}$Zr), and finally to γ-unstable ($^{106-110}$Zr).

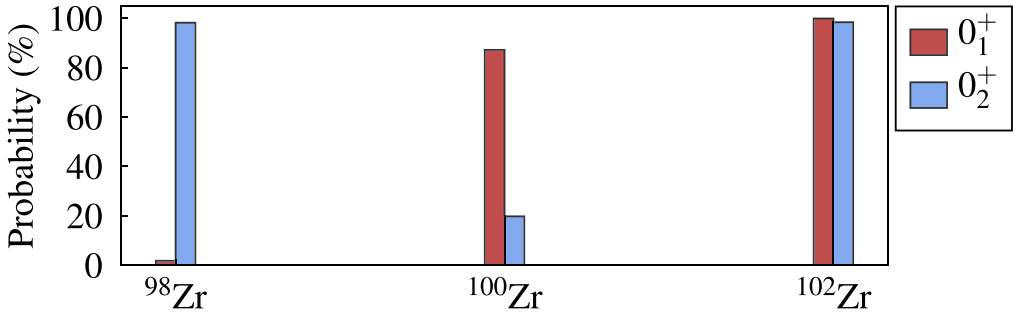

Figure 5. Percentage of the wave functions within the intruder B-configuration [the b^2 probability in equation (12)], for the ground (0_1^+) and excited (0_2^+) states in ^{98}Zr, ^{100}Zr and ^{102}Zr.

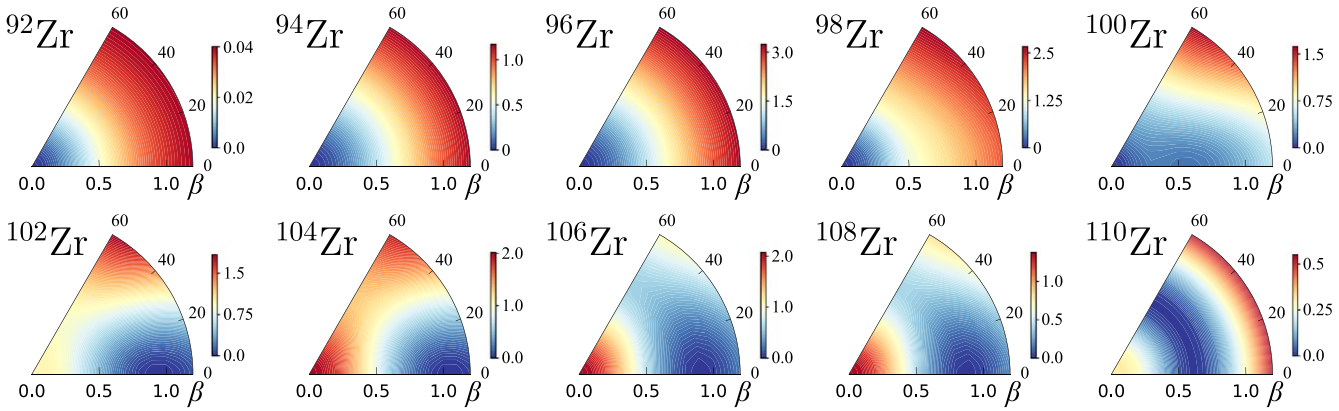

Figure 6. Contour plots in the (β, γ) plane of the lowest eigen-potential surface, $E_{-}(\beta, \gamma)$, for the $^{92-110}$Zr isotopes, obtained from diagonalizing the matrix (8) with entries given in equation (14).

5. Evolution of energy levels

An important clue for understanding the change in structure of the Zr isotopes, is obtained by examining the evolution of their spectra along the chain. In figure 7, we show a comparison between experimental and calculated levels, along with assignments to configurations based on equation (12), and to the closet DS for each level. One can see here a rather complex structure. In the region between neutron number 50 and 56, there appear to be two configurations, one spherical (seniority-like), (A), and one weakly deformed, (B), as evidenced by the ratio $R_{4/2}$ in each configuration which is at 52–56, $R_{4/2}^{(A)} \cong 1.6$ and $R_{4/2}^{(B)} \cong 2.3$. From neutron number 58, there is a pronounced drop in energy for the states of configuration (B), and at 60, the two configurations exchange their roles. This is evident in figure 5 from the change in the decomposition of the ground state 0_1^+ from configuration A ($a^2 = 98.2\%$) in ^{98}Zr, to configuration B ($b^2 = 87.2\%$) in ^{100}Zr. The 0_2^+ state displays the opposite trend, changing from configuration B in ^{98}Zr ($b^2 = 98.2\%$) to configuration A ($a^2 = 80.2\%$) in ^{100}Zr. At this stage, the intruder configuration (B) appears to be at the critical point of a U(5)-SU(3) QPT, as evidenced in figures 4(c) and (d), by the low value of the excitation energy of the 0_3^+ state in ^{100}Zr, which is the first excited 0^+ state of the B-configuration ($b^2 = 92.9\%$). The spectrum of states in this configuration resembles that of the X(5) critical-point symmetry [49]. The same situation is seen in the $_{62}$Sm and $_{64}$Gd isotopes at neutron number 90 [25, 51]. In ^{102}Zr, that state becomes the first excited 0_2^+ state and serves as the band-head of a β-band. Interestingly, the change in configurations appears sooner in the 2_1^+ level, which changes to configuration B ($b^2 = 97.1\%$) already in ^{98}Zr, as pointed out in [17]. In general, beyond neutron number 60, the intruder configuration (B) becomes progressively strongly deformed, as evidenced by the small value of the excitation energy of the state 2_1^+, $E_{2_1^+} = 151.78$ keV and by the ratio $R_{4/2}^{(B)} = 3.15$ in ^{102}Zr, and $E_{2_1^+} = 139.3$ keV, $R_{4/2}^{(B)} = 3.24$ in ^{104}Zr. At still larger neutron number 66, the ground state band becomes γ-unstable (or triaxial) as evidenced by the close energy of the states 2_2^+ and 4_1^+, $E_{2_2^+} = 607.0$ keV, $E_{4_1^+} = 476.5$ keV, in ^{106}Zr, and especially by the recent results $E_{4_1^+} = 565$ keV and $E_{2_2^+} = 485$ keV in ^{110}Zr [16], a signature of the SO(6) symmetry. In this region, the ground state configuration undergoes a crossover from SU(3) to SO(6).

6. Evolution of order parameters and related observables

The above spectral analysis suggests a remarkable interplay of configurations-interchange and shape-evolution in the Zr isotopes, manifesting simultaneously two types of QPTs. The first type of QPT involves an abrupt crossing of the normal

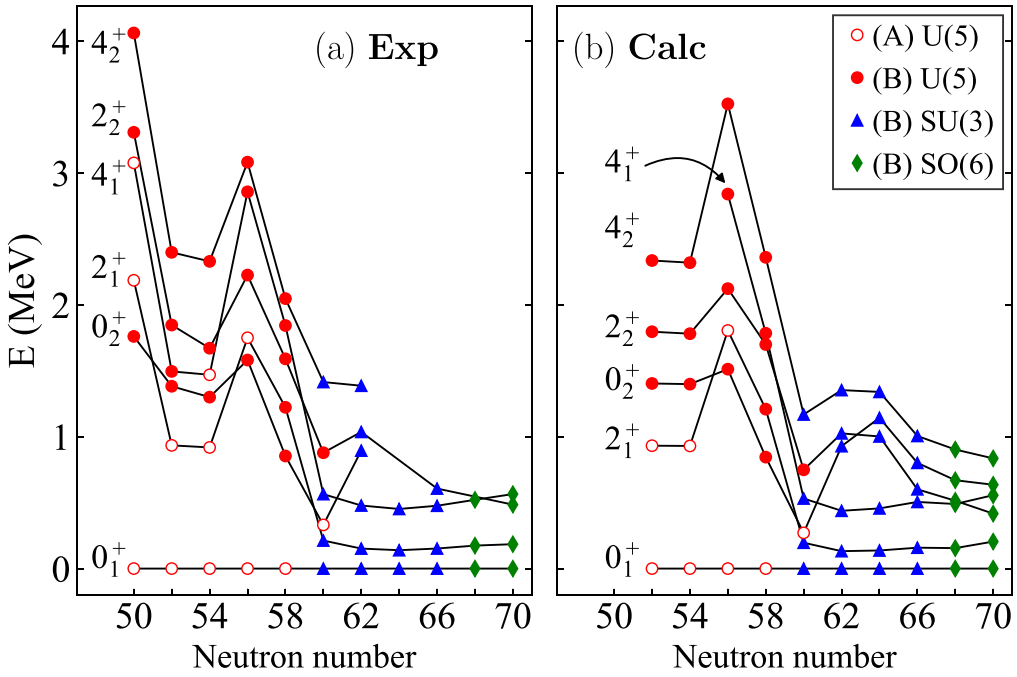

Figure 7. Comparison between (a) experimental [16, 50] and (b) calculated energy levels 0_1^+, 2_1^+, 4_1^+, 0_2^+, 2_2^+, 4_2^+. Empty (filled) symbols indicate a state dominated by the normal A-configuration (intruder B-configuration), with assignments based on the decomposition of equation (12). The shape of the symbol [$\circ$, $\triangle$, $\Diamond$], indicates the closest DS [U(5), SU(3), SO(6)] relevant to the level considered. Note that the calculated values start at neutron number 52, while the experimental values include the closed shell at 50.

and intruder configurations. A second type of QPT involves a gradual shape change of the intruder configuration which undergoes a first-order U(5) to SU(3) transition and an SU(3) to SO(6) crossover. In order to understand the nature of these phase transitions, one needs to study the behavior of the order parameters. In the present study, the latter involve the expectation value of $\hat{n}_d$ in the ground state wave function, $|\Psi; L = 0_1^+\rangle$ and in its Ψ_A and Ψ_B components (12), denoted by $\langle \hat{n}_d \rangle_{0_1^+}$, $\langle \hat{n}_d \rangle_A$, $\langle \hat{n}_d \rangle_B$, respectively. As can be inferred from equation (3), $\langle \hat{n}_d \rangle_A$ and $\langle \hat{n}_d \rangle_B$ portray the shape-evolution in configuration (A) and (B), respectively. $\langle \hat{n}_d \rangle_{0_1^+}$ involves a sum of these quantities weighted by the probabilities of the Ψ_A and and Ψ_B components,

$$\langle \hat{n}_d \rangle_{0_1^+} = a^2 \langle \hat{n}_d \rangle_A + b^2 \langle \hat{n}_d \rangle_B, \tag{15}$$

hence contains information on the normal-intruder mixing in $|\Psi; L = 0_1^+\rangle$.

Figure 8(a) shows the evolution along the Zr chain of these order parameters ($\langle \hat{n}_d \rangle_A$, $\langle \hat{n}_d \rangle_B$ in dotted and $\langle \hat{n}_d \rangle_{0_1^+}$ in solid lines), normalized by the respective boson numbers, $\langle \hat{N} \rangle_A = N$, $\langle \hat{N} \rangle_B = N + 2$, $\langle \hat{N} \rangle_{0_1^+} = a^2 N + b^2 (N + 2)$. Configuration ($A$) is seen to be spherical for all neutron numbers considered. In contrast, configuration (B) is weakly-deformed for neutron number 52–58. One can see here clearly a jump between neutron number 58 and 60 from configuration (A) to configuration (B), indicating a first-order configuration-changing phase transition, a further increase at neutron numbers 60–64 indicating a U(5)-SU(3) shape-phase transition within configuration (B), and, finally, there is a decrease at neutron number 66, due in part to the crossover from SU(3) to SO(6) and in part to the shift from boson particles to boson holes after the middle of the major shell 50–82. $\langle \hat{n}_d \rangle_{0_1^+}$ is close to $\langle \hat{n}_d \rangle_A$ for neutron number 52–58 and coincides with $\langle \hat{n}_d \rangle_B$ at 60 and above, consistent with a high degree of purity with respect to configuration-mixing.

The above conclusions are stressed by an analysis of other observables, in particular, the $B(E2)$ values. As shown in figure 8(b), the calculated $B(E2)$'s agree with the empirical values and follow the same trends as the respective order parameters. The dotted lines denote calculated $E2$ transitions between states within the same configuration. The calculated $2_A^+ \rightarrow 0_A^+$ transition rates coincide with the empirical $2_1^+ \rightarrow 0_1^+$ rates for neutron number 52–56. The calculated $2_B^+ \rightarrow 0_B^+$ transition rates coincide with the empirical $2_2^+ \rightarrow 0_2^+$ rates for neutron number 52–56, with the empirical $2_1^+ \rightarrow 0_2^+$ rates at neutron number 58, and with the empirical $2_1^+ \rightarrow 0_1^+$ rates at neutron number 60–64. The large jump in $B(E2; 2_1^+ \rightarrow 0_1^+)$ between neutron number 58 and 60 reflects the passing through a critical point, common to a QPT involving a crossing of two configurations and a spherical to deformed U(5)-SU(3) type of QPT within the B-configuration. The further increase in $B(E2; 2_1^+ \rightarrow 0_1^+)$ for neutron numbers 60–64 is as expected for a U(5)-SU(3) QPT within configuration (B) (see figure 2.20 in [25]) and, as in figure 8(a), reflects an increase in the deformation in a spherical to deformed shape-phase transition. The subsequent decrease from the peak at neutron number 64 towards 70, is in accord with an SU(3) to SO(6) crossover (see figure 2.22 in [25]).

In general, the results of the current phenomenological study resemble those obtained in the microscopic approach of

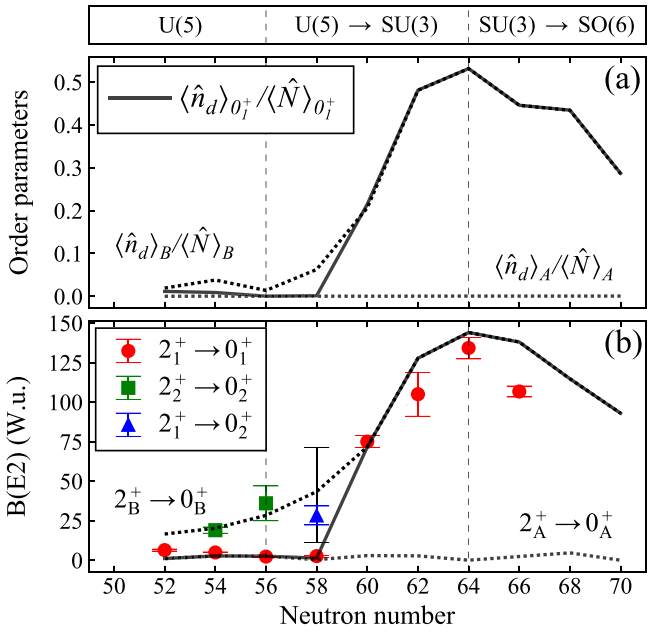

Figure 8. Evolution of order parameters and of observables along the Zr chain. Symbols (solid lines) denote experimental data (calculated results). (a) The order parameters are the calculated expectation values of $\hat{n}_d$ in the total ground state wave function $|\Psi; L = 0_1^+\rangle$, equation (12) and in its (A) and (B) components (dotted lines), normalized by the respective boson numbers. (b) $B(E2)$ values in Weisskopf units (W.u.). Data taken from [12–15, 17, 18, 50]. Dotted lines denote calculated $E2$ transitions within a configuration.

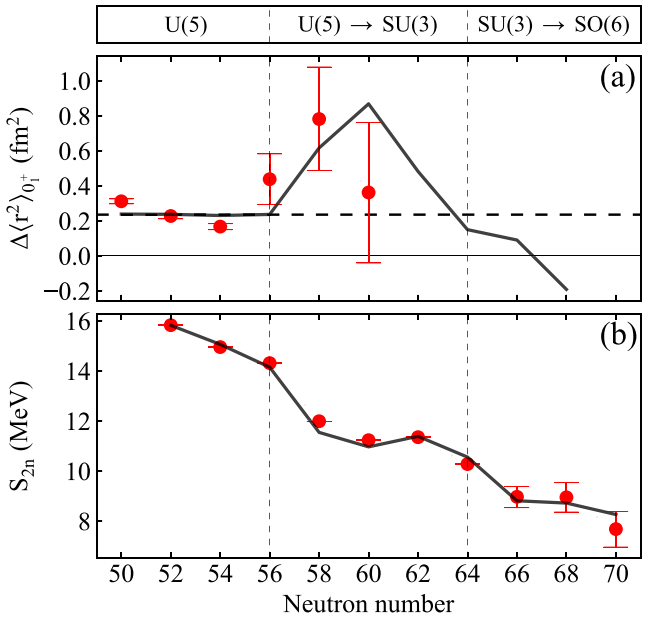

Figure 9. Evolution of observables along the Zr chain. Symbols (solid lines) denote experimental data (calculated results). (a) Isotope shift, $\Delta\langle\hat{r}^2\rangle_{0_1^+}$ in fm^2. Data taken from [54]. The horizontal dashed line at 0.235 fm^2 represents the smooth behavior in $\Delta\langle\hat{r}^2\rangle_{0_1^+}$ due to the $A^{1/3}$ increase of the nuclear radius. (b) Two-neutron separation energies, S_{2n}, in MeV. Data taken from AME2016 [55].

the MCSM [11] (which focuses on spectra and $E2$ rates), however, there are some noticeable differences. Specifically, the replacement γ-unstable $\to$ triaxial and the inclusion of more than two configurations in the MCSM. The spherical state in ^{100}Zr is identified in the MCSM as 0_4^+, in contrast to 0_2^+ in the current calculation and the data. Both calculations show a large jump in $B(E2; 2_1^+ \to 0_1^+)$, between ^{98}Zr and ^{100}Zr, typical of a first-order QPT. This is in contrast with mean-field based calculations [6–8], which due to their character smooth out the phase transitional behavior, and show no such jump at the critical point of the QPT (see figure 2 of [18]). The observed peak in $B(E2; 2_1^+ \to 0_1^+)$ for ^{104}Zr, is reproduced by the current calculation but not by the MCSM.

Further evidence for the indicated structural changes occurring in the Zr chain, can be obtained from an analysis of the isotope shift $\Delta\langle\hat{r}^2\rangle_{0_1^+} = \langle\hat{r}^2\rangle_{0_1^+;A+2} - \langle\hat{r}^2\rangle_{0_1^+;A}$, where $\langle\hat{r}^2\rangle_{0_1^+}$ is the expectation value of $\hat{r}^2$ in the ground state 0_1^+. In the IBM-CM the latter is given by

$$\langle\hat{r}^2\rangle = r_c^2 + \alpha N_\nu + \eta[\langle\hat{n}_d^{(N)}\rangle + \langle\hat{n}_d^{(N+2)}\rangle], \tag{16}$$

where r_c^2 is the square radius of the closed shell, N_ν is half the number of valence particles, and η is a coefficient that takes into account the effect of deformation [25, 52, 53]. The isotope shift depends on two parameters, $\alpha = 0.235$, $\eta = 0.264$ fm^2, whose values are fixed by the procedure of [52, 53]. $\Delta\langle\hat{r}^2\rangle_{0_1^+}$ should increase at the transition point and decrease and, as seen in figure 9(a), it does so, although the error bars are large and no data are available beyond neutron number 60. (In the large N limit, this quantity, proportional to the derivative of the order parameter $\langle\hat{n}_d\rangle_{0_1^+}$, diverges at the critical point.)

Similarly, the two-neutron separation energies S_{2n} can be written as [25],

$$S_{2n} = -\tilde{A} - \tilde{B}N_\nu \pm S_{2n}^{\rm def} - \Delta_n, \tag{17}$$

where $S_{2n}^{\rm def}$ is the contribution of the deformation, obtained by the expectation value of the Hamiltonian in the ground state 0_1^+. The + sign applies to particles and the − sign to holes, and Δ_n takes into account the neutron subshell closure at 56, $\Delta_n = 0$ for 50–56 and $\Delta_n = 2$ MeV for 58–70. The value of Δ_n is taken from table XII of [56] and $\tilde{A} = -16.5$, $\tilde{B} = 0.758$ MeV are determined by a fit to binding energies of ^{92,94,96}Zr. The calculated S_{2n}, shown in figure 9(b), displays a complex behavior. Between neutron number 52 and 56 it is a straight line, as the ground state is spherical (seniority-like) configuration (A). After 56, it first goes down due to the subshell closure at 56, then it flattens as expected from a first-order QPT (see, for example the same situation in the $_{62}$Sm isotopes [51]). After 62, it goes down again due to the increasing of deformation and finally it flattens as expected from a crossover from SU(3) to SO(6).

7. Conclusions

We have presented here a quantum analysis of spectra and other observables (including $E2$ rates, isotope shifts, separation energies) and a classical analysis of shapes, for the entire

chain of $_{40}$Zr isotopes, from neutron number 52 to 70. The calculations were performed within the IBM-CM, which provides a simple tractable shell-model-inspired algebraic framework, where global trends of structure and symmetries can be clearly identified and diversity of observables calculated. The evolution of structure and QPT attributes, along the Zr chain, are studied by varying the control parameters in the IBM-CM Hamiltonian followed by a detailed comparison with the available experimental data on yrast and non-yrast states.

The results of the comprehensive analysis suggest a complex phase structure in these isotopes, involving two configurations. The normal *A* configuration remains spherical in all isotopes considered. The intruder *B*-configuration undergoes first a spherical to axially-deformed U(5)-SU(3) QPT, with a critical-point near ^{100}Zr, and then an axially-deformed to γ-unstable SU(3)-SO(6) crossover. In parallel to the gradual shape-evolution within configuration *B*, the two configurations cross near neutron number 60, and the ground state changes from configuration (*A*) to configuration (*B*). Interestingly, the critical-point of the U(5)-SU(3) shape-changing QPT coincides with the critical-point of the configuration-changing QPT. The two configurations are weakly mixed and retain their purity before and after the crossing.

Further details of our results, including the calculation of spectra and transition rates in all the $^{92-110}$Zr isotopes and of other quantities not reported here, will be given in a forthcoming publication based on [48]. Our method of calculation could also be applied to the $_{38}$Sr isotopes, which show similar features [57]. The present work provides the first evidence for multiple QPTs in nuclear physics and may stimulate research for this type of phase transitions in other fields of physics.

Acknowledgments

This work was supported in part by US DOE under Grant No. DE-FG02-91ER-40608 and by the US-Israel Binational Science Foundation Grant No. 2016032. We thank R F Casten and J E García-Ramos for insightful discussions and for bringing to our attention a recently reported IBM-CM calculation for the Zr isotopes [58], which conforms with the results of the present analysis.

References

[1] Cheifetz E R, Jared C, Thompson S G and Wilhelmy J B 1970 *Phys. Rev. Lett.* **25** 38
[2] Federman P and Pittel S 1977 *Phys. Lett.* B **69** 385
[3] Federman P and Pittel S 1979 *Phys. Rev.* C **20** 820
[4] Heyde K, Van Isacker P, Casten R and Wood J L 1985 *Phys. Lett.* B **155** 303
[5] Heyde K and Wood J L 2011 *Rev. Mod. Phys.* **83** 1467
[6] Delaroche J P, Girod M, Libert J, Goutte H, Hilaire S, Péru S, Pillet N and Bertsch G F 2010 *Phys. Rev.* C **81** 014303
[7] Nomura K, Rodríguez-Guzmán R and Robledo L M 2016 *Phys. Rev.* C **94** 044314
[8] Mei H, Xiang J, Yao J M, Li Z P and Meng J 2012 *Phys. Rev.* C **85** 034321
[9] Sieja K, Nowacki F, Langanke K and Martínez-Pinedo G 2009 *Phys. Rev.* C **79** 064310
[10] Petrovici A 2012 *Phys. Rev.* C **85** 034337
[11] Togashi T, Tsunoda Y, Otsuka T and Shimizu N 2016 *Phys. Rev. Lett.* **117** 172502
[12] Chakraborty A *et al* 2013 *Phys. Rev. Lett.* **110** 022504
[13] Browne F *et al* 2015 *Phys. Lett.* B **750** 448
[14] Kremer C *et al* 2016 *Phys. Rev. Lett.* **117** 172503
[15] Ansari S *et al* 2017 *Phys. Rev.* C **96** 054323
[16] Paul N *et al* 2017 *Phys. Rev. Lett.* **118** 032501
[17] Witt W *et al* 2018 *Phys. Rev.* C **98** 041302
[18] Singh P *et al* 2018 *Phys. Rev. Lett.* **121** 192501
[19] Gilmore R and Feng D H 1978 *Phys. Lett.* B **76** 26
[20] Gilmore R 1979 *J. Math. Phys.* **20** 891
[21] Carr L 2011 *Understanding Quantum Phase Transitions* (Boca Raton, FL: CRC Press)
[22] Cejnar P, Jolie J and Casten R F 2010 *Rev. Mod. Phys.* **82** 2155
[23] Heyde K, Jolie J, Fossion R, De Baerdemacker S and Hellemans V 2004 *Phys. Rev.* C **69** 54304
[24] Gavrielov N, Leviatan A and Iachello F 2019 *Phys. Rev.* C **99** 064324
[25] Iachello F and Arima A 1987 *The Interacting Boson Model* (Cambridge: Cambridge University Press)
[26] Iachello F and Talmi I 1987 *Rev. Mod. Phys.* **59** 339
[27] Ginocchio J N and Kirson M W 1980 *Phys. Rev. Lett.* **44** 1744
[28] Dieperink A E L, Scholten O and Iachello F 1980 *Phys. Rev. Lett.* **44** 1747
[29] Cejnar P and Jolie J 2009 *Prog. Part. Nucl. Phys.* **62** 210
[30] Iachello F 2011 *Riv. Nuovo Cimento* **34** 617
[31] Warner D D and Casten R F 1983 *Phys. Rev.* C **28** 1798
[32] Lipas P O, Toivonen P and Warner D S 1985 *Phys. Lett.* B **155** 295
[33] Duval P D and Barrett B R 1981 *Phys. Lett.* B **100** 223
[34] Duval P D and Barrett B R 1982 *Nucl. Phys.* A **376** 213
[35] Sambataro M and Molnár G 1982 *Nucl. Phys.* A **376** 201
[36] Duval P D, Goutte D and Vergnes M 1983 *Phys. Lett.* B **124** 297
[37] Padilla-Rodal E, Castaños O, Bijker R and Galindo-Uribarri A 2006 *Rev. Mex. Fis.* S **52** 57
[38] Fossion R, Heyde K, Thiamova G and Van Isacker P 2003 *Phys. Rev.* C **67** 024306
[39] Frank A, Van Isacker P and Iachello F 2006 *Phys. Rev.* C **73** 061302
[40] García-Ramos J E, Hellemans V and Heyde K 2011 *Phys. Rev.* C **84** 14331
[41] García-Ramos J E and Heyde K 2014 *Phys. Rev.* C **89** 14306
[42] García-Ramos J E and Heyde K 2015 *Phys. Rev.* C **92** 034309
[43] Nomura K, Otsuka T and Van Isacker P 2016 *J. Phys. G: Nucl. Part. Phys.* **43** 024008
[44] Leviatan A, Gavrielov N, García-Ramos J E and Van Isacker P 2018 *Phys. Rev.* C **98** 031302
[45] Frank A, Van Isacker P and Vargas C E 2004 *Phys. Rev.* C **69** 034323
[46] Hellemans V, Van Isacker P, De Baerdemacker S and Heyde K 2007 *Nucl. Phys.* A **789** 164
[47] Heyde K, Jolie J, Moreau J, Ryckebusch J, Waroquier M, Duppen P V, Huyse M and Wood J L 1987 *Nucl. Phys.* A **466** 189
[48] Gavrielov N *PhD Thesis* The Hebrew University
[49] Iachello F 2001 *Phys. Rev. Lett.* **87** 052502
[50] Evaluated Nuclear Structure Data File (ENSDF) (https://nndc.bnl.gov/ensdf/)
[51] Scholten O, Iachello F and Arima A 1978 *Ann. Phys.* **115** 325
[52] Zerguine S, Van Isacker P, Bouldjedri A and Heinze S 2008 *Phys. Rev. Lett.* **101** 022502

[53] Zerguine S, Van Isacker P and Bouldjedri A 2012 *Phys. Rev.* C **85** 034331
[54] Angeli I and Marinova K P 2013 *At. Data Nucl. Data Tables* **99** 69
[55] Wang M, Audi G, Kondev F G, Huang W, Naimi S and Xu X 2017 *Chin. Phys.* C **41** 030003
[56] Barea J and Iachello F 2009 *Phys. Rev.* C **79** 044301
[57] Mach H, Moszynnski M, Gill R, Wohn F, Winger J, C Hill J, Molnár G and Sistemich K 1989 *Phys. Lett.* B **230** 21
[58] García Ramos J E and Heyde K 2019 (arXiv:1909.00824 [nucl-th])